Applied Catalysis B: Environmental 339 (2023) 123075

Contents lists available at ScienceDirect

Applied Catalysis B: Environmental

journal homepage: www.elsevier.com/locate/apcatb

High-loaded single-atom Cu-N_3 sites catalyze hydrogen peroxide decomposition to selectively induce singlet oxygen production for wastewater purification

Fuhang Xu [a,b], Cui Lai [a,b,*], Mingming Zhang [a,b], Bisheng Li [c], Ling Li [a,b], Shiyu Liu [a,b], Dengsheng Ma [a,b], Xuerong Zhou [a,b], Huchuan Yan [a,b], Xiuqin Huo [a,b], Biting Wang [a,b], Huan Yi [a,b], Lei Qin [a,b], Lin Tang [a,b]

[a] College of Environmental Science and Engineering, Hunan University, Changsha 410082, Hunan, PR China
[b] Key Laboratory of Environmental Biology and Pollution Control (Hunan University), Ministry of Education, Changsha 410082, Hunan, PR China
[c] College of Geography and Environmental Sciences, Zhejiang Normal University, Jinhua 321004, Zhejiang, PR China

ARTICLE INFO

Keywords:
H_2O_2-based Fenton-like
Singlet oxygen
High-load Cu single-atom catalyst
Cu-N_3 sites

ABSTRACT

Single-atom catalysts (SACs) have been widely used in Fenton-like water treatment, but studies on the selective induction of H_2O_2 to produce singlet oxygen ($^1O_2$) are rare. Herein, a carbon nitride supported high-loaded single-atom Cu-N_3 catalyst (Cu-CN, Cu load is 15.46 wt%) is prepared to activate H_2O_2 to selectively form $^1O_2$. Experimental and DFT calculation results reveal that the key factor for $^1O_2$ production is the Cu-N_3 coordination structure. Specifically, Cu-N_3 coordination structure is conducive to decomposing H_2O_2 into·OOH/·O_2^-. Besides, the density of Cu-N_3 sites is another key factor, high Cu-N_3 site density is conducive to the rapid conversion of·OOH/·O_2^- to $^1O_2$. Benefitting from the dominant role of $^1O_2$, the Fenton-like degradation performance of Cu-CN/ H_2O_2 system is not disturbed under high salinity conditions, and the performance is significantly enhanced at high pH. This work represents an important reference in understanding SACs for activated H_2O_2 to generate $^1O_2$.

1. Introduction

With the rapid development of society, there are more and more refractory organic pollutants (such as dyes, antibiotics, personal care products, and pesticides) in domestic and industrial wastewater [1,2]. These organic pollutants not only cause persistent threats to the ecological environment and human health, but also bring new challenges to sewage treatment [3]. For these difficult-to-biodegrade organic pollutants, advanced oxidation processes (AOPs), which rely on the highly reactive oxygen species (ROS) to degrade and mineralize organic pollutants, are considered to be effective treatment technologies [4–6]. Unfortunately, radical-based AOPs are easily obstructed by inorganic salt ions, which will scavenge radical or produce more toxic secondary pollutants [7]. Furthermore, radical-based AOPs are generally limited to acidic condition [8]. Therefore, in the face of wastewater with high salinity and alkalinity (such as textile, chemical, paper, food, and pharmaceutical wastewater, etc.), the removal efficiency of radical-based AOPs is not ideal.

Recently, nonradical pathways such as singlet oxygen ($^1O_2$) oxidation, electron transfer process (ETP), and high-valent metal-induced oxidation process have attracted much attention in water treatment [9–11]. Nonradical-dominated catalytic systems can resist the molestation of high salinity in wastewater to maintain their excellent efficiency in complex water matrices [12,13]; they do not produce toxic halogen-containing products even in the existence of high concentrations of halide ions [14]. Therefore, nonradical-based heterogeneous AOPs are considered to be promising methods for the purification of high salinity and alkaline wastewater.

Currently, single-atom catalysts (SACs) with both homogeneous and heterogeneous advantages are considered to be ideal heterogeneous Fenton-like catalysts [15–19]. Furthermore, many studies have confirmed that SACs have great potential in inducing nonradical oxidation pathway dominated by $^1O_2$ [20–23]. However, the research is mainly focused on the activation of persulfate (PS). Although PS

* Corresponding author at: College of Environmental Science and Engineering, Hunan University, Changsha 410082, Hunan, PR China.
E-mail address: laicui@hnu.edu.cn (C. Lai).

https://doi.org/10.1016/j.apcatb.2023.123075
Received 15 April 2023; Received in revised form 11 June 2023; Accepted 5 July 2023
Available online 13 July 2023

activation is considered to be a new favorite for water treatment due to its low cost, ease of storage and transportation [24], it cannot be ignored that when PS is used for water treatment, sulfate is inevitably introduced, resulting in new environmental risks. Hydrogen peroxide (H_2O_2), by contrast, is cleaner, environmentally friendly and does not introduce additional salt ions. However, at present, H_2O_2-based AOPs mainly take hydroxyl radical (·OH) as the main oxidation species and have strict pH requirements, so the performance is inhibited in high salinity and alkaline wastewater. To expand the applicability of H_2O_2-based AOPs, it is necessary to develop efficient Fenton-like catalysts that can catalyze H_2O_2 to selectively induce $^1O_2$ production for wastewater purification. However, at present, the selective generation of $^1O_2$ by activation of H_2O_2 over SACs is rarely studied. The structure-activity relationship between the structural characteristics of SACs and the efficient conversion of H_2O_2 to $^1O_2$ is not clear. Therefore, it is significant to study the efficient and highly selective production of $^1O_2$ by activating H_2O_2 via SACs.

Analysis of the process of converting H_2O_2 to $^1O_2$ (H_2O_2 →·OOH/·O_2^- → $^1O_2$) [25], from the view of electron transfer, the generation of the key intermediates (·OOH/·O_2^-) needs electron transfer from H_2O_2 to the catalyst. However, during the activation of H_2O_2 by transition metals, the reaction rate of H_2O_2 loss electrons to generate·OOH/·O_2^- is often much lower than the rate of gain electrons to generate ·OH [26,27]. Consequently, to realize the highly selective conversion of H_2O_2 to $^1O_2$, the conversion of H_2O_2 to·OOH/·O_2^- needs to be enhanced first. In the study of the activation of PS by SACs to produce $^1O_2$, it was found that SACs with metal-N-C (M-N-C) structure, due to their unique electronic configuration, can enhance transfer electrons from PS to metal sites to form $^1O_2$ [28–30]. Inspired by this, the electron loss process of H_2O_2 may occur more easily on SACs with M-N-C structure, which is favorable to activate H_2O_2 to·OOH/·O_2^-. Moreover, the conversion of·OOH/·O_2^- to $^1O_2$ is dependent on oxidation by metal sites or the recombination of radicals. When the metal active sites are dense, the·OOH/·O_2^- generated on the metal sites can rapidly contact with the neighboring metal sites or the radicals generated on the neighboring metal sites, thus rapidly converting to $^1O_2$. Therefore, we speculate that high-loaded SACs with M-N-C structure may be able to efficiently activate H_2O_2 and selectively generate $^1O_2$.

Herein, carbon nitride (CN) supported Cu single-atom catalyst (Cu-CN) with M-N-C structure was used as a heterogeneous catalyst for H_2O_2 activation. The characterization results proved that Cu-CN was successfully synthesized and had Cu-N_3 coordination structure. The experimental results showed that Cu-CN/H_2O_2 Fenton-like systems followed nonradical pathway dominated by $^1O_2$, and exhibited excellent activity in pollutant degradation even under high salinity and alkaline conditions. Based on the experimental and DFT calculation results, the reasons of Cu-CN selectively converting H_2O_2 to $^1O_2$ were analyzed in detail. Furthermore, the effect of Cu site density on the catalytic pathway of Cu-CN/H_2O_2 Fenton-like system was revealed. Although Cu SACs with Cu-N-C structure have been reported for determination, production, and activation of H_2O_2 [30–33], it is rare to report that Cu-CN SACs can activate H_2O_2 to selectively generate $^1O_2$. This work provides an important reference and new idea for the design of SACs for activating H_2O_2 to generate $^1O_2$, and promotes the development of SACs applied to H_2O_2-activated nonradical-based AOPs.

2. Experimental

The details of the relevant chemicals, catalyst synthesis, characterizations and analysis methods involved in the experiment are provided in the Supporting Information, Text S1 −S6.

3. Results and discussion

3.1. Characteristics

The microscopic morphologies of Cu-CN were characterized by transmission electron microscopy (TEM). As shown in Fig. 1a, Cu-CN exhibits a lamellar stacking structure of nanoflakes, which is basically consistent with the structure of CN monomer (Fig. S1), connoting that the introduction of Cu atoms does not change the microscopic morphology of CN. In addition, no lattice fringes and metal nanoparticles such as metallic Cu or CuO are observed in the high-resolution TEM (HR-TEM) images of Cu-CN, indicating the amorphous structural composition of Cu-CN. Additionally, Cu-CN was observed by high-angle annular dark-field scanning transmission electron microscopy (HAADF-STEM), which further determines the existence form of Cu. Fig. 1**d** shows the presence of very distinct dense but isolated bright spots, indicating that Cu atoms exist in a single-atom state and the loading of Cu single atom is very high in Cu-CN. The actual content of Cu in Cu-CN is 15.46% by inductively coupled plasma optical emission spectrometer (ICP-OES) measurement, indicating the high loading of Cu single atom. Moreover, Fig. S2 presents the HAADF-STEM diagrams of Cu-CN with different Cu loading amounts. Cu single atom are uniformly dispersed on Cu-CN0.5, and the density is lower than that of Cu-CN. As for Cu-CN1.5, Cu clusters formed by excessive aggregation of Cu atoms and the lattice stripes belonging to CuO can be observed. In Fig. 1e, elemental mapping energy dispersive X-ray spectroscopy (EDS) also demonstrates that the Cu atoms uniformly distributed on the CN matrix.

Fig. 2a shows the X-ray diffraction (XRD) patterns of CN and Cu-CN. The XRD pattern of Cu-CN is generally consistent with CN, and no diffraction peaks of any other Cu-based substances are detected, which is conformable to the results of TEM. The elemental chemical states of Cu-CN were analyzed by X-ray photoelectron spectroscopy (XPS). Comparing the N 1 s and C 1 s spectra of CN and Cu-CN (Fig. S3), no obvious difference is observed, indicating that the loading of Cu single atom does not affect the formation of CN. In addition, compared with CN, the N 1 s spectrum of Cu-CN shift slightly towards the high binding energy, which could be attributed to the interaction between pyridine N and Cu atoms, leading to a slight decrease in electron density of N atom [34]. For the Cu 2p spectrum of Cu-CN, two obvious splitting peaks (934.42 eV and 932.68 eV) are observed at Cu $2p_{3/2}$ (Fig. 2b), which could be attributed to Cu (II) and Cu(I), respectively [31]. Additionally, the result of modified Auger parameter (α', the sum of the kinetic energy of Cu-LMM Auger electron and the binding energy of Cu $2p_{3/2}$ photoelectron, Cu(0): α' = 1851.0 eV, Cu(I): α' = 1849.0 eV [35]) further confirms that the peak of the reduced state (932.68 eV) belongs to Cu(I) rather than Cu(0). Combining the Cu LMM Auger spectrum (insert of Fig. 2b), the value of α' is 1848.03 eV (915.35 eV plus 932.68 eV) close to that of Cu(I), which further confirms the absence of Cu(0). Furthermore, Cu K-edge extended X-ray absorption fine structure spectroscopy (EXAFS) was used to explore the fine structure of Cu atoms in Cu-CN. From Fig. 2c, the absorption edge of Cu in Cu-CN is sandwiched between the absorption edge of CuO and Cu_2O, indicating that the valence state of Cu atoms was located between + 1 and + 2. This further demonstrates that Cu (II) and Cu (I) coexist in Cu-CN, which is consistent with the results of XPS. Fig. 2d displays the Fourier transform of the Cu K-edge EXAFS of the Cu-CN catalyst. The spectrum of Cu-CN is significantly different from that of Cu, Cu_2O, and CuO. As for Cu-CN, only one major peak at ≈ 1.49 Å is presented, corresponding to Cu-N coordination [31,36,37]. Furthermore, the characteristic peak of Cu-Cu coordination cannot be observed in Cu-CN, indicating the absence of metallic crystalline Cu species and the presence of Cu species in the form of single-atom dispersion. Additionally, it can be obtained from the EXAFS fitting curve for the first shell in the k-space and R-space (Fig. 2e-f and Table S1) that the average coordination number of Cu-N is 3. The above characterization results reveal that Cu in Cu-CN existed in single-atom form dispersion and is stabilized by Cu-N_3 coordination, which

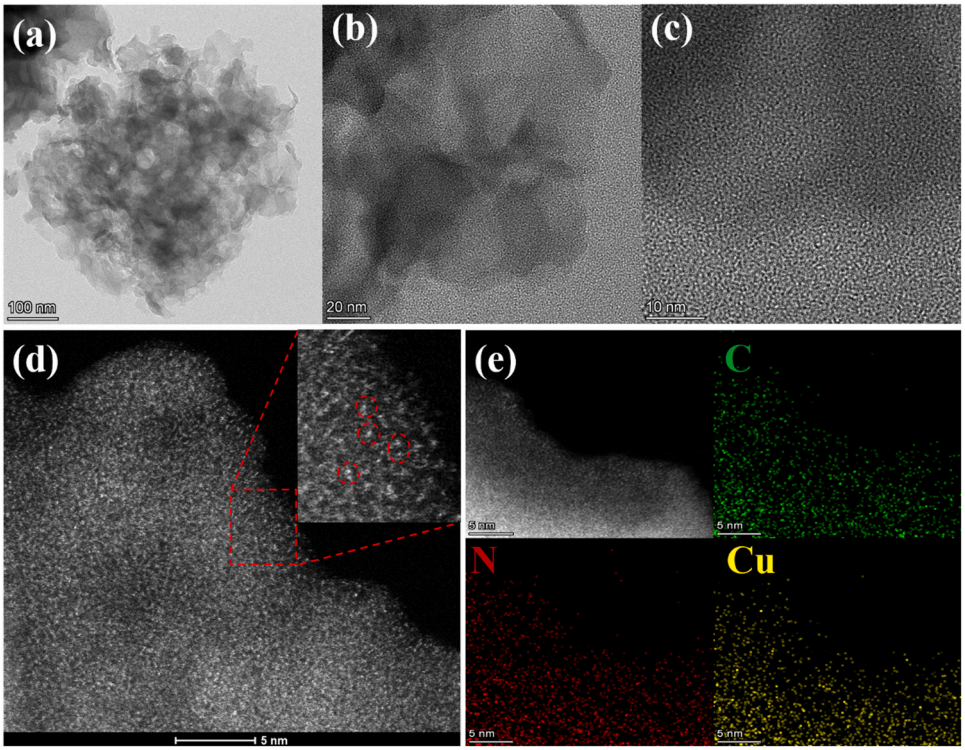

Fig. 1. (a, b) TEM and (c) HRTEM images of CuCN. (d) HAADF-STEM image and (e) HAADF mapping images of CuCN.

confirms the successful synthesis of Cu-CN.

3.2. Fenton-like activity

The Fenton-like properties and mechanism of H_2O_2 activation by Cu-CN were evaluated by degrading methylene blue (MB) in aqueous solution. As shown in Fig. 3a, MB is hardly degraded by H_2O_2 alone, and the degradation rate of MB is only 2.57% within 40 min. Then, the Fenton-like performance of Cu-CN with pure CN, traditional Cu-containing catalyst (CuO, Cu_2O), and homogeneous Cu^{2+} (the concentration of Cu^{2+} is consistent with the total Cu content of Cu-CN/H_2O_2/MB Fenton-like system, that is, the concentration of Cu^{2+} = 0.3 g/L×15.46% = 0.046 g/L) were compared. In the Cu-CN/MB system without H_2O_2 addition, the concentration of MB does not change within 20 min, manifesting that the adsorption equilibrium has been reached and very little MB was removed by adsorption. Besides, the Fenton-like performance of Cu-CN is much higher than the CN, CuO, Cu_2O and homogeneous Cu^{2+}, the removal rate of MB can reach 93.6% within 40 min, and the TOC removal efficiency is 34.64%. The quasi-first-order rate constant (k) of Cu-CN is 0.0712 min^{-1}, which is 17 times, 6 times, 14.5 times, and 5.6 times of CN (0.0042 min^{-1}), CuO (0.0119 min^{-1}), Cu_2O (0.0049 min^{-1}), and Cu^{2+} (0.0127 min^{-1}), respectively (Fig. 3b, Table S2). Furthermore, the normalized k based on metal molar amount ($k_{per\text{-}mol\ Cu}$), specific surface area ($k_{surface\text{-}area}$), and turnover frequency (TOF) are calculated (Table S3) [38]. Compared with other catalysts, Cu-CN has the highest $k_{per\text{-}mol\ Cu}$ (98.34 $min^{-1}mol^{-1}$), $k_{surface\text{-}area}$ (2.25 $\times10^{-3}$ min^{-1} $(m^2)^{-1}g$), and TOF value (1.01 $\times10^{-3}$ min^{-1}), indicating the better Fenton-like performance. The TOF value of Cu-CN is also compared with other previously reported Cu-based Fenton-like catalysts in Table S4. The results show that the Fenton-like performance of Cu-CN is better than that of most previously reported Cu-based catalysts. In addition, as shown in Fig. S4, with the decrease of Cu content, the activity of the catalyst decreased obviously, indicating that Cu atoms are the main active sites. However, when the content of Cu is excessive, the catalytic performance is inhibited, which is due to the formation of Cu clusters and CuO (Fig. S2), confirming that the single-atom-dispersed Cu sites have a better catalytic performance.

3.3. Active species and catalytic mechanism of Cu-CN/H_2O_2 Fenton-like system

Active species quenching experiments were performed to determine the main active species produced in Cu-CN/H_2O_2 system. Tert-butyl alcohol (TBA) and 1,4-Benzoquinone (BQ) were used as quenching agents for ·OH and $\cdot O_2^-$, respectively, and furfuryl alcohol (FFA) and L-tryptophan were used as quenching agents for $^1O_2$ [39,40]. According to Fig. 3c, the addition of TBA and BQ has no significant effect on the degradation of MB, signifying that ·OH and $\cdot O_2^-$ are not the main active species. Namely, the Fenton-like degradation of MB in Cu-CN/H_2O_2 system does not follow the traditional radical pathway. Meanwhile, both FFA and L-tryptophan significantly inhibited the degradation of MB, indicating that $^1O_2$ is the main active species. To further determine the existence of $^1O_2$ in the Cu-CN/H_2O_2 Fenton-like system, the probe method was used for identification (1,3-Diphenylisobenzofuran (DPBF) was used as the molecular probe for $^1O_2$) [41]. Specifically, the absorption peak of DBPF at 411 nm gradually decreased with the passage of reaction time (Fig. 3d), indicating the production of $^1O_2$ during the reaction. In addition, the active species in Cu-CN/H_2O_2/MB Fenton system were further identified by electron spin resonance (EPR) technique. As shown in Fig. 3e, no obvious ·OH signal is observed. Besides, a weak $\cdot O_2^-$ signal and strong $^1O_2$ signal appeared. This indicates that ·OH and $\cdot O_2^-$ in the system can be ignored, and the main active species is $^1O_2$, which is consistent with the results of quenching experiments. Furthermore, the ROS generated in Cu-CN/H_2O_2/MB system were quantitatively determined [29]. $^1O_2$ accounted for 93.38% of all ROS, indicating a highly selective conversion of H_2O_2 to $^1O_2$ (Fig. S5).

Meanwhile, in addition to $^1O_2$, the nonradical pathway may also include ETP and high-valent metal-induced oxidation process [10,42,43]. Therefore, some electrochemical tests were carried out to verify the contribution of ETP in MB degradation. The LSV curves (Fig. 3f) exhibit that the current of Cu-CN/H_2O_2 is significantly higher than that of Cu-CN, indicating obvious electron transfer exists between H_2O_2 and

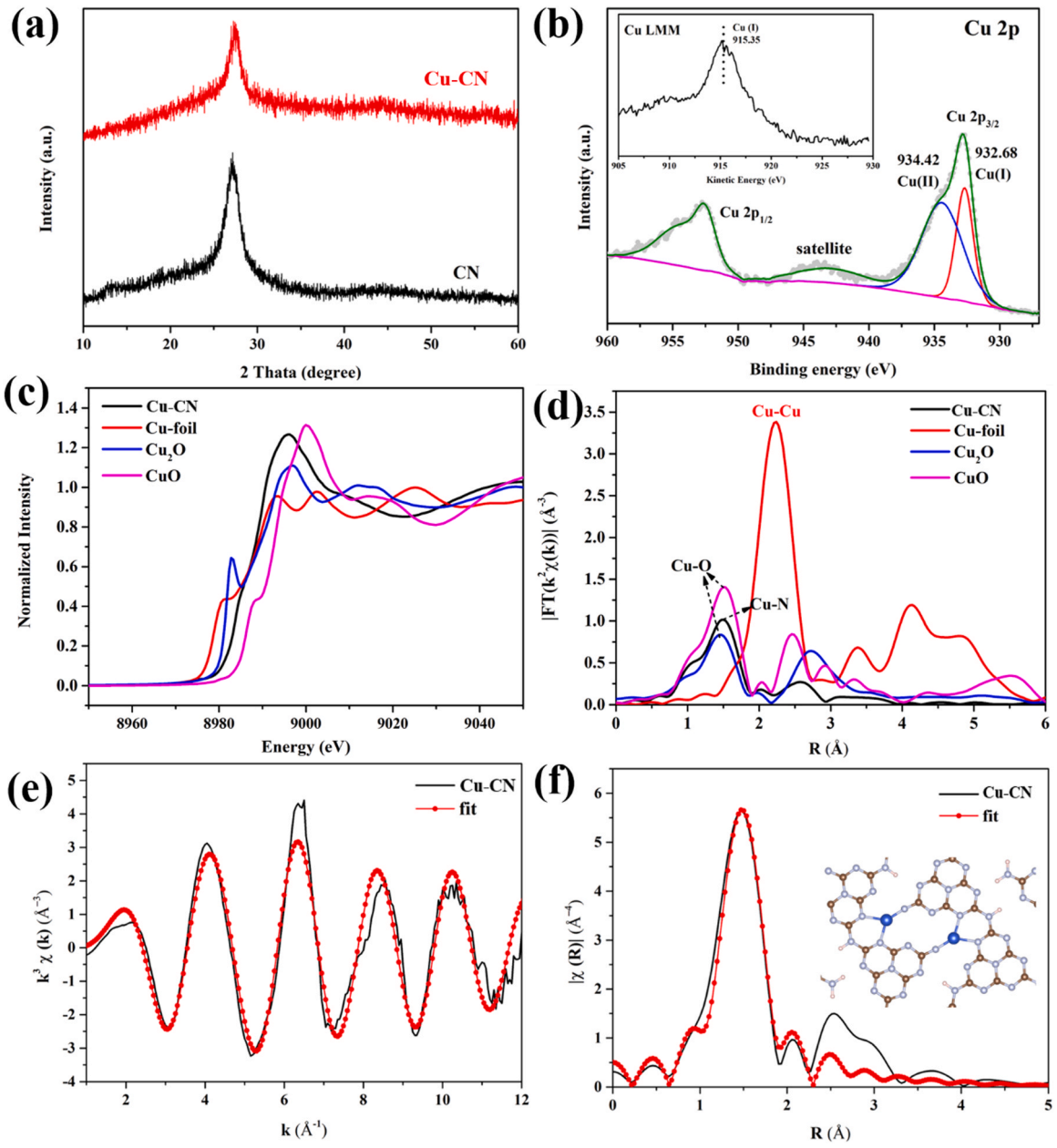

Fig. 2. (a) XRD patterns of CN and Cu-CN. (b) XPS Cu 2p spectrum and Cu LMM Auger spectrum (inset) of Cu-CN. (c) Cu K-edge XANES and (d) Fourier transform of the Cu K-edge EXAFS of Cu-CN and reference samples Cu foil, Cu_2O, and CuO; Fitting curves of the EXAFS of Cu atom of Cu-CN in the (e) k-space and (f) R-space.

Cu-CN. However, the curve of Cu-CN/H_2O_2/MB shows no difference with Cu-CN/H_2O_2, indicating that no electron transfer occurred between MB and Cu-CN/H_2O_2, insinuating that there is no ETP pathway for MB degradation. Furthermore, the open-circuit potential (OCP) tests (Fig. 3g) show a significant increase in potential after the addition of H_2O_2, which is due to the formation of the complex of the catalyst and H_2O_2. However, the potential did not decrease with the subsequent addition of MB, indicating that no direct electron transfer process occurred between MB and catalyst surface [44]. In addition, in the salt bridge primary cell experiment (Fig. S6) the current is only 1.4 μA after adding H_2O_2 and gradually decreased over time, and MB has no apparent degradation in the primary cell, which further confirms that MB degradation by ETP pathway is negligible. Additionally, the generation of high-valent Cu (Cu (III)) in the catalytic process was identified by in situ Raman (Fig. 3h). The characteristic peak of Raman spectrum around 615 cm^{-1} can be used as a basis for identification of Cu (III) species [45,46]. It is observed that the characteristic peak of Cu (III) near 615 cm^{-1} is not found after the addition of H_2O_2, indicating that Cu (III) is not formed in the Fenton-like process, which excluded high-valent metal-induced oxidation. To sum up, it can be concluded that the catalytic mechanism of Cu-CN/H_2O_2/MB Fenton-like system is dominated by the nonradical paths of $^1O_2$, which is different from the traditional Fenton-like mechanism that is dominated by the generation of ·OH.

3.4. *The formation mechanism of $^1O_2$*

To further understand the activation mechanism of H_2O_2 by Cu-CN, the formation mechanism of $^1O_2$ is then discussed in detail. According to Fig. S7, O_2 does not affect the degradation of MB, suggesting that the only source of $^1O_2$ is H_2O_2. The generation of $^1O_2$ from H_2O_2 can go through a two-step one-electron path. Hence, based on the previous researches and Haber-Weiss cycle [25,47,48], a possible two-step one-electron path from H_2O_2 to $^1O_2$ is proposed as follows (Fig. 4). The first one-electron path can be described as the formation of

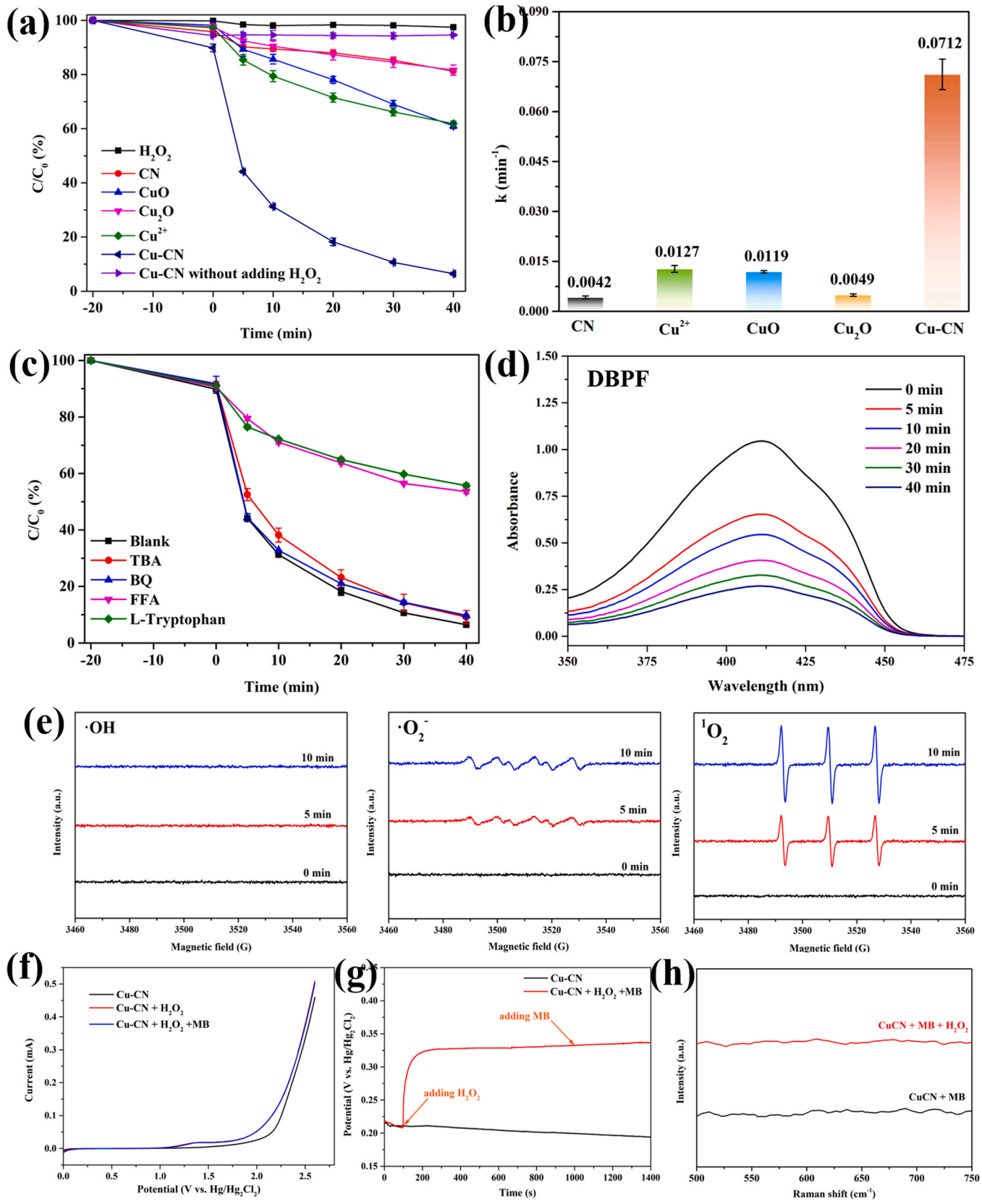

Fig. 3. (a) Degradation curves of MB and (b) the pseudo-first-order kinetic constant (k) in different Fenton-like systems. (c) Quenching experiments for degradation of MB in Cu-CN/H_2O_2 Fenton-like systems. (d) Absorption spectra of DBPF with reaction time in Cu-CN/H_2O_2 Fenton-like system. (e) EPR spectra of·OH,·O_2^-, and $^1O_2$ in Cu-CN/H_2O_2/MB systems. (f) Linear sweep voltammetry curves of Cu-CN after adding H_2O_2 and MB. (g) Open-circuit potential versus time curves. (h) In situ Raman spectra of the CuCN/H_2O_2/MB systems.

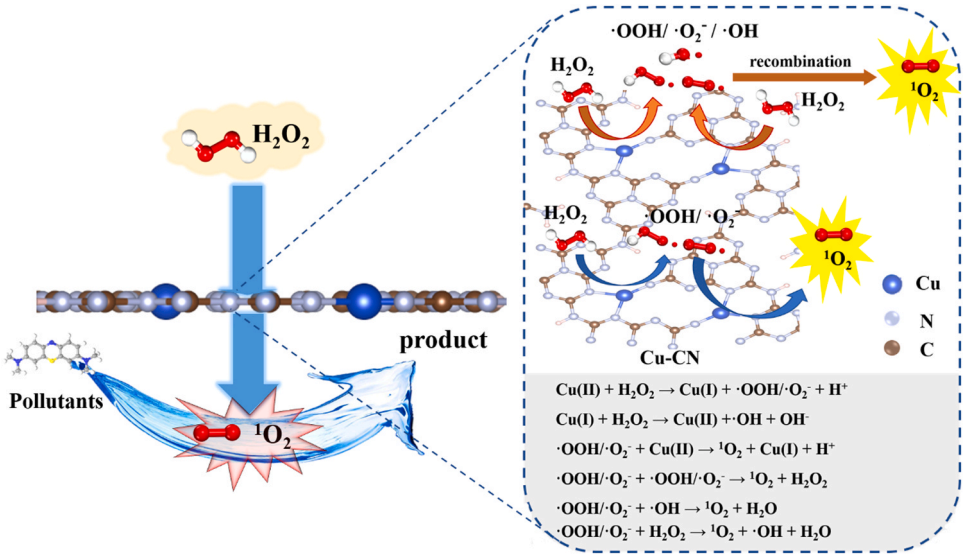

Fig. 4. Mechanism diagram of the Cu-CN/H_2O_2 system for MB removal.

$HO_2{\cdot}/{\cdot}O_2^-$ through the reaction between H_2O_2 and Cu-CN (Eq. 3). To be specific, when H_2O_2 combines with Cu(II), H_2O_2 can transfer one electron to Cu(II) to form Cu(I) and $HO_2{\cdot}$(Eq. 1) [49], and $HO_2{\cdot}$can be further dissociated into${\cdot}O_2^-$ (Eq. 2) [50]. The second one-electron transfer path is the further oxidation of $HO_2{\cdot}/{\cdot}O_2^-$ to $^1O_2$, including three possible pathways. The first pathway is that the generated $HO_2{\cdot}/{\cdot}O_2^-$ is rapidly oxidized by the adjacent Cu(II) sites (Eq. 4), and the high density of Cu (II) sites in Cu-CN in conductive to the occurrence of this reaction. The second route is the recombination of free radicals. The generated $HO_2{\cdot}/{\cdot}O_2^-$ can spontaneously recombine with itself or·OH to generate $^1O_2$, (Eq. 5 and Eq. 6) [25,47,48]. Although the ESR and quenching experiments show the absence of·OH, the generation of·OH is inevitable considering the reaction between Cu(I) and H_2O_2 (Eq. 7) [49]. Besides, the existence of·OH is not detected by the quenching experiments and EPR may be attributed to the slow diffusion of the quencher and the rapid recombination of·OH with adjacent radicals [51]. For the third pathway, according to the classical Haber-Weiss reaction, $HO_2{\cdot}/{\cdot}O_2^-$ can react with H_2O_2 to form $^1O_2$ (Eq. 8) [25,52].

$$Cu(II) + H_2O_2 \rightarrow Cu(I) + {\cdot}OOH + H^+ \quad (1)$$

$${\cdot}OOH \rightarrow {\cdot}O_2^- + H^+ \quad (2)$$

$$Cu(II) + H_2O_2 \rightarrow Cu(I) + {\cdot}OOH/{\cdot}O_2^- + H^+ \quad (3)$$

$$Cu(II) + {\cdot}OOH/{\cdot}O_2^- \rightarrow Cu(I) + {}^1O_2 + H^+ \quad (4)$$

$${\cdot}OOH/{\cdot}O_2^- + {\cdot}OOH/{\cdot}O_2^- \rightarrow {}^1O_2 + H_2O_2 \quad (5)$$

$${\cdot}OOH/{\cdot}O_2^- + {\cdot}OH \rightarrow {}^1O_2 + H_2O \quad (6)$$

$$Cu(I) + H_2O_2 \rightarrow Cu(II) + {\cdot}OH + OH^- \quad (7)$$

$${\cdot}OOH/{\cdot}O_2^- + H_2O_2 \rightarrow H_2O + {\cdot}OH + {}^1O_2 \quad (8)$$

3.5. Relationship between catalyst structure and $^1O_2$ formation

According to the reported literature, Cu-based catalysts always generate·OH rapidly when activating H_2O_2 since $k_1 < k_7$ ($k_1 = 4.6 \times 10^2$ $M^{-1}s^{-1}$, $k_7 = 1 \times 10^4$ $M^{-1}s^{-1}$) [53], while the generation of $HO_2{\cdot}/{\cdot}O_2^-$, which is the key procedure for $^1O_2$ generation, is usually very slow. Due to the lack of $HO_2{\cdot}/{\cdot}O_2^-$, the rapidly generated·OH will react directly with pollutants. Therefore, conventional Cu-based Fenton-like systems follow an·OH dominated radical pathway. As shown in Fig. S8, the addition of TBA into Cu^{2+}/H_2O_2 and CuO/H_2O_2 Fenton-like systems almost completely suppressed the degradation of MB, indicating that·OH plays a dominant role, which is distinct from the Cu-CN/H_2O_2 system. This difference implies that single-atom Cu sites with Cu-N-C structure may be more susceptible to the Eq. 1 to generate·OOH.

DFT calculation was used to further verify that Cu-CN is more likely to generate·OOH compared to conventional Cu-based catalysts (taking CuO as an example) when H_2O_2 is activated. Firstly, based on the results of EXAFS, a CuCN model with Cu-N_3 coordination configuration is constructed (Fig. 5a). The average bond length of Cu-N (1.915 Å) with structural optimization is basically consistent with the fitting results of EXAFS (1.970±0.062 Å) (Table S2). Then, the differential charge density of Cu-CN is calculated (Fig. 5b), and an obvious charge transfer around Cu-N_3 can be found, indicating that Cu-N_3 is the main active site for redox reaction. Furthermore, the adsorption and activation processes of H_2O_2 on Cu-CN are calculated to explore the activation mechanism of H_2O_2 by Cu-CN, and the (111) face of CuO is used as a contrast. Besides, to fully consider the effects of different sites and orientations of H_2O_2 on the catalyst surface, three different initial models are constructed (Fig. 5c). The calculation results show that the H_2O_2 with different initial positions were all adsorbed on the Cu site (Fig. S9), indicating that the Cu site was the main adsorption site of H_2O_2. And the three models all showed negative adsorption energy (−2.34 eV, −2.35 eV, and −2.27 eV) for H_2O_2, indicating that the adsorption of H_2O_2 by Cu-CN was thermodynamically favorable. Besides, all three models show that the length of O-O bond of H_2O_2 adsorbed on Cu-CN was shorter than that of free H_2O_2 (1.483 Å), which may be disadvantageous to the breaking of O-O bond. The free energy of two activation paths of H_2O_2 (H_2O_2→·OOH, H_2O_2→·OH) on Cu-CN and CuO were calculated (Fig. 5c). All models show that the energy barrier for the conversion of H_2O_2 to·OH is much higher than that for·OOH on Cu-CN, indicating that the conversion to·OOH has more thermodynamic advantages. On the contrary, the energy barrier for the conversion of H_2O_2 to·OH on CuO is much lower than that of·OOH, which makes it more inclined to generate·OH. Based on the above DFT calculation results, it is known that compared with the traditional Cu-based catalysts, Cu-CN is easier to activate H_2O_2 to·OOH, which makes the key reaction for the formation of $^1O_2$ easier to occur. These results explained why $^1O_2$ rather than·OH is the main active species in the Cu-CN/H_2O_2 Fenton-like system.

Although based on the above analysis, it is concluded that one of the vital factors that CuCN can selectively induce H_2O_2 to generate $^1O_2$ is that the Cu-N_3 structure is easier to convert H_2O_2 into the key intermediate (·OOH/$\cdot O_2^-$) of $^1O_2$, it still cannot explain why the radicals

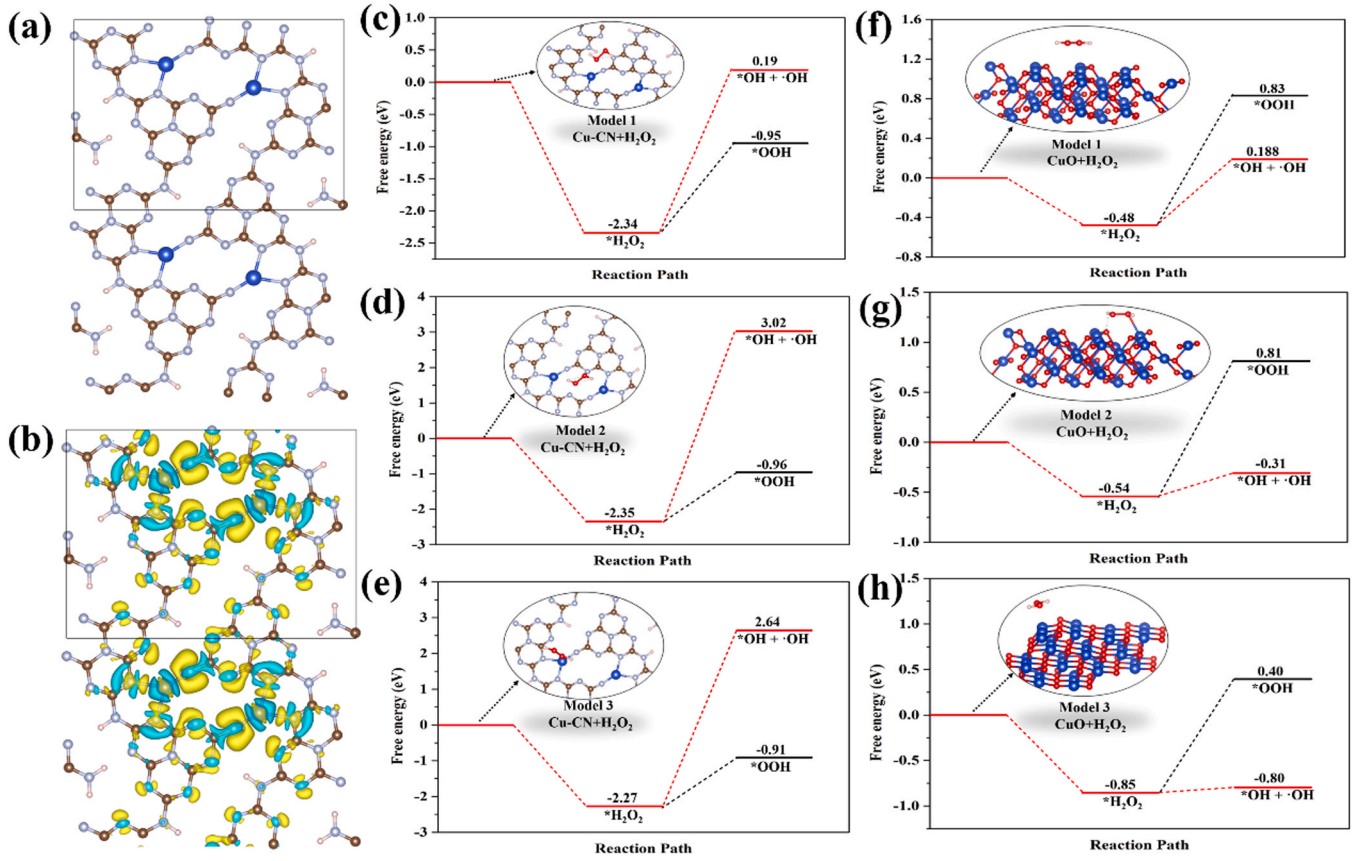

Fig. 5. (a) Optimized atomic structure of Cu-CN. (b) Electron density differences of the top view for Cu-CN (the yellow regions represent electron-rich and the blue represent electron-defective). Free energy diagrams for generating ·OOH and ·OH on (c-e) Cu-CN and (f-h) CuO.

(·OOH/·O_2^-/·OH) generated by activated H_2O_2 do not directly participate in the degradation of pollutants but preferentially further convert into $^1O_2$. Therefore, there should be another key factor in Cu-CN that makes the generated radicals rapidly converted into $^1O_2$ rather than contacting with pollutants. From the mechanism of H_2O_2 to produce $^1O_2$, we speculate that the density of Cu-N_3 sites may be another key factor affecting the Fenton-like catalytic mechanism of Cu-CN. To verify this hypothesis, the effect of the density of Cu-N_3 sites in Cu-CN on its Fenton-like catalytic mechanism was explored. Cu-CN with different Cu-N_3 site densities were obtained by changing the addition amount of Cu $(NO_3)_2{\cdot}3\ H_2O$ in the synthesis process (Cu-CN0.5 and Cu-CN0.25 corresponding to the addition amount of 0.5 mmol and 0.25 mmol of Cu $(NO_3)_2{\cdot}3\ H_2O$, respectively). As shown in Fig. S10,·OH could be detected in both Cu-CN0.5/H_2O_2 and Cu-CN0.25/H_2O_2 systems. Furthermore, the contribution of different active species to the degradation of MB in Cu-CN0.5/H_2O_2/MB and Cu-CN0.25/H_2O_2/MB system was analyzed by quenching experiment (Fig. S11). Since BQ had no inhibitory effect on the degradation of MB, the inhibitory effect of TBA on the degradation of MB was used to estimate the contribution of the radical oxidation pathway. According to the results (Fig. 6a), the density of Cu-N_3 site significantly affect the proportion of active species, and it follows a certain rule, that is, the contribution of·OH-based radical pathway gradually decreased with the increase of Cu-N_3 site density. As a result, low Cu-N_3 sites density tends to increase the proportion of radical pathways dominated by·OH, which may be due to the large distance between the Cu-N_3 site is not conducive to the formation of $^1O_2$. Specifically, when the density of Cu-N3 sites was low, the radicals generated on the active sites were far away from the adjacent Cu(II) sites or radicals, so it was not conducive to the further oxidation of·OOH/·O_2^- by Cu (II) and the recombination of radicals, thereby limiting the generation of $^1O_2$. Conversely, the high density of Cu-N_3 sites creates a condition for the rapid conversion of radicals (·OOH/·O_2^-/·OH) to $^1O_2$, which is another key that Cu-CN can selectively induce H_2O_2 to produce $^1O_2$. Moreover, the current response and electrochemical impedance of Cu-CN with different Cu-N_3 sites density in the presence of H_2O_2 were also tested. It is observed from Fig. 6b-c that the current response is significantly enhanced and the electrochemical impedance is significantly reduced with the increase of Cu-N_3 sites density. This confirms that high Cu-N_3 site density is conducive to the electron transfer between catalyst and H_2O_2. Generally, the formation of $^1O_2$ is closely related to the electron transfer between H_2O_2 and Cu-CN, thus the facilitation of electron transfer between H_2O_2 and Cu-CN by the high Cu-N_3 site density can also be conducive to the generation of $^1O_2$. The finding of the effect of Cu-N_3 sites density on active species has a certain guiding significance for designing single-atom catalysts with controllable active species, but its more detailed internal mechanism remains to be further investigated.

3.6. *Fenton-like performance of Cu-CN under high-salinity alkaline wastewater*

In order to examine the performance of Cu-CN/H_2O_2 Fenton-like system in complex wastewater, high-salinity alkaline wastewater was prepared. Referring to the previous research [54], the composition of the high-salinity alkaline wastewater used in the experiment is shown in Table 1. Surprisingly, the degradation of MB was not inhibited but significantly promoted under high salinity conditions (Fig. 7a), which deviated from the traditional H_2O_2-based Fenton-like catalysis. To further verify the high degradation performance of CuCN/H_2O_2 system under high-salinity alkaline conditions, the degradation performance of other common industrial dyes (RhB and MO) was tested (Fig. 7b, Fig. S12). As expected, RhB and MO were degraded effectively even

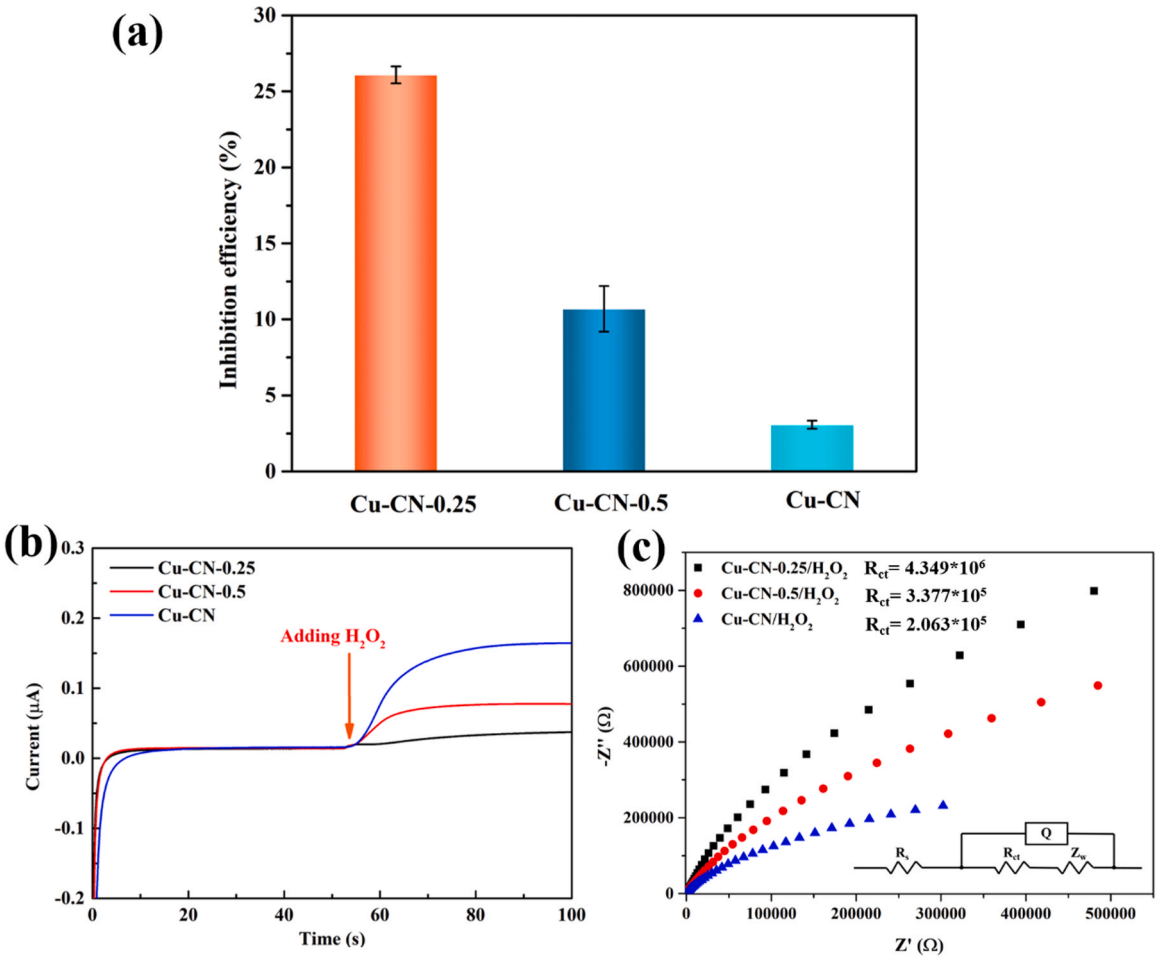

Fig. 6. (a) Inhibition of quenching radicals on MB degradation under different Cu site densities (Reaction conditions: [TBA]=100 mM; [MB]=31.3 μM; [H_2O_2]= 30 mM); (b) Current responses and (c) electrochemical impedance spectroscopy of CuCN-0.25, CuCN-0.5, and CuCN with adding H_2O_2.

Table 1
The composition of synthetic high-salinity alkaline wastewater.

Species	Molar concentration (mol L^{-1})	Mass Concentration (g L^{-1})
NaCl	0.06	3.51
Na_2SO_4	0.015	2.13
KCl	0.04	2.98
NH_4OH	0.25	8.76
NaH_2PO_4	0.0136	1.63
NH_4HCO_3	0.25	19.77
pH	9	

under high-salinity alkaline conditions. Similar to MB, the degradation of MO was enhanced, while the degradation of RhB was slightly inhibited. This is because RhB is an anionic dye, and the enhancement of surface negative electricity of CuCN in the alkaline condition is adverse to the adsorption of RhB. Fortunately, this inhibition is not obvious, and still maintains a high degradation efficiency. These results fully demonstrate the superiority of the CuCN/H_2O_2 Fenton-like system in treating high-salinity alkaline wastewater, and the excellent performance may be attributed to the dominant role of $^1O_2$ during catalytic reaction.

To further explore the reasons for the enhancement of degradation under high-salinity alkaline, the possible influencing factors were analyzed one by one. As for solution pH (Fig. 7c), it can be observed that the degradation of MB was significantly promoted with the increase of pH. This may be because the increase of OH^- concentration in the solution was beneficial to the positive progress of Eq. 1, Eq. 2, Eq. 3, and Eq. 4. Therefore, the increase of pH in solution was beneficial to the formation of $^1O_2$. In addition, the obvious inhibition of the reaction when pH was 3 and 4 is also related to the surface charge of Cu-CN. Zeta potential test shows that the surface of Cu-CN is positively charged when pH ≤ 4 (Fig. S13), which is not conducive to the retention of positively charged MB on the catalyst surface. In general, various anions in high-salinity alkaline wastewaters also have an effect on Fenton-like catalytic activity, so the effect of each anion was evaluated here (the concentration of the tested ion was consistent with the total concentration of the ion in Table 1.). As shown in Fig. 7d, Cl^- and SO_4^{2-} almost had no effect on the degradation of MB. Meanwhile, both HCO_3^- and CO_3^{2-} promoted the degradation of MB, and the promotion degree of CO_3^{2-} is higher than that of HCO_3^- and the pH of CO_3^{2-} is also higher than that of HCO_3^- (Fig. 7e). While the degradation of MB is significantly inhibited by $H_2PO_4^-$, but markedly promoted by HPO_4^{2-}. By measuring the variation of solution pH after addition of anions (Fig. 7e), it is found that the addition of CO_3^{2-}, HCO_3^-, HPO_4^{2-} increased solution pH, and the solution containing CO_3^{2-} had the highest pH value. Meanwhile, the presence of $H_2PO_4^-$ decreased the solution pH. Combined with the results of pH effect in Fig. 7a, it can be concluded that carbonate ions and phosphate ions can affect the activity of CuCN/H_2O_2 Fenton-like system by changing the solution pH. To further verify this inference, we studied the effects of Cl^-, NO_3^-, SO_4^{2-}, NO_2^-, HCO_3^-, and $H_2PO_4^-$ under the same pH conditions (Fig. S14). In order to eliminate the effect of pH, HNO_3 and NaOH were used to adjust the pH of solutions containing NO_2^-, HCO_3^-, and $H_2PO_4^-$. The results show that the effects of Cl^-, NO_3^-, and SO_4^{2-} on the degradation of MB at both low and high concentrations are negligible. NO_2^-, HCO_3^-

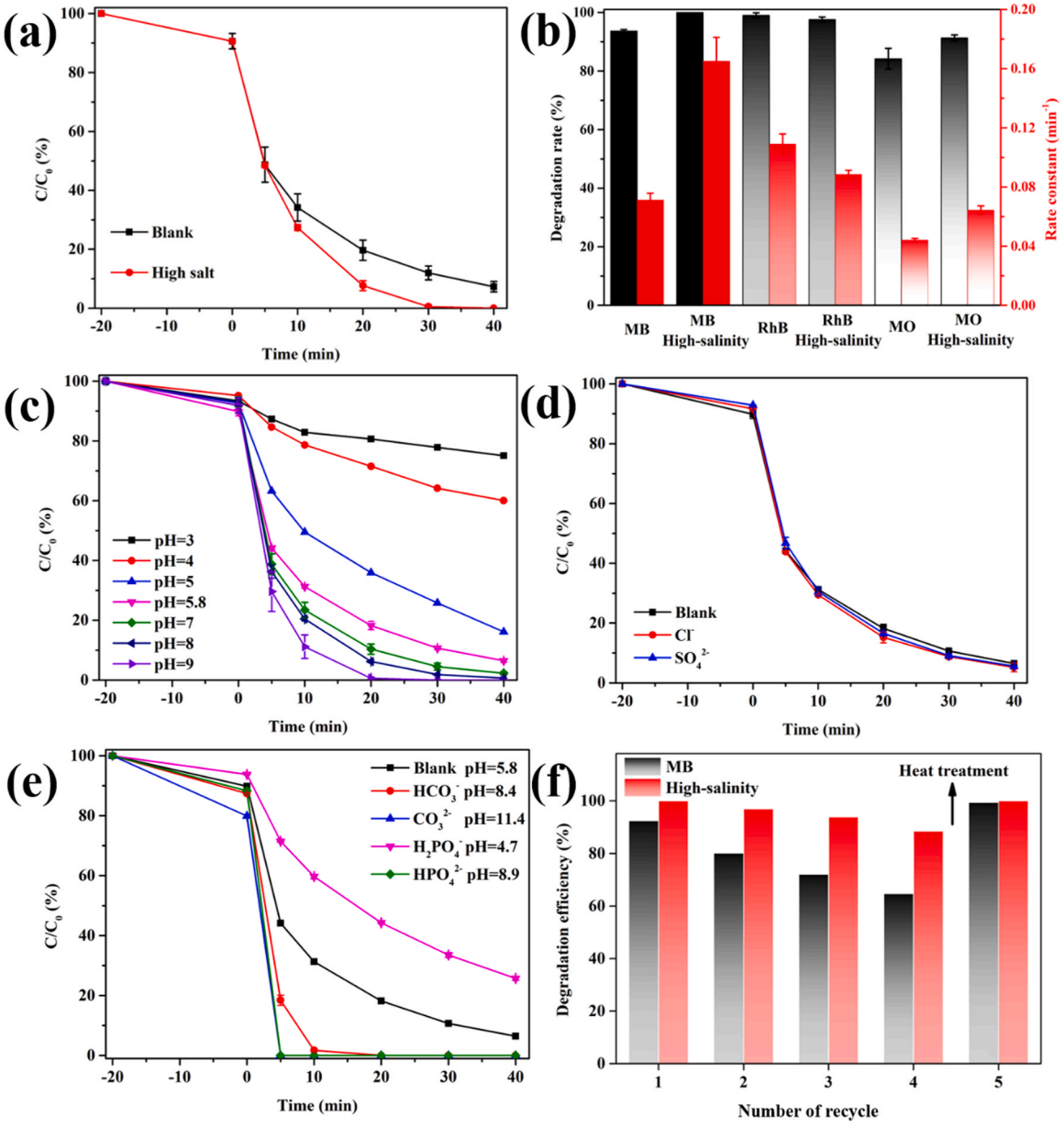

Fig. 7. (a) Degradation curve of MB by Cu-CN/H_2O_2 Fenton-like system under high-salinity alkaline condition. (b) Degradation rate and quasi-first-order Kinetic constant of MB, MO, RhB by Cu-CN/H_2O_2 system under high-salinity alkaline condition. (c) The effects of initial pH, and (d, e) anions on the degradation of MB. (f) Cyclic performance of Cu-CN/H_2O_2 Fenton-like system.

and $H_2PO_4^-$ has obvious effects on MB degradation, but these effects are consistent with the effect of solution pH on MB degradation. After adjusting the solution to the same pH, no significant effect on the degradation of MB, confirming that the Cu-CN/H_2O_2/MB system is not disturbed by inorganic ions, but affected by pH. This characteristic of Cu-CN/H_2O_2 Fenton-like system makes it have great potential in the treatment of high saline-alkaline wastewater.

3.7. Adaptability and stability of Cu-CN

The effects of humic acid and different water bodies on MB degradation were discussed to further investigate the adaptability of the Cu-CN/H_2O_2 system in complex water quality. Even at high humic acid concentration (40 mg L^{-1}), the degradation of MB was only slightly inhibited (Fig. S15), indicating that humic acid had little interference to Cu-CN/H_2O_2 system. As exhibited in Fig. S16, the Cu-CN/H_2O_2/MB system also showed excellent performance in actual water bodies. The degradation efficiencies of MB in tap water, lake water, and Xiangjiang River water are enhanced, which can be attributed to their pH is higher than that of ultrapure water. Additionally, the stability of Cu-CN was investigated by cycling experiments, both under high salt and non-salt systems. The results were shown in Fig. 7f, the catalytic performance of Cu-CN decreased in both systems after each cycle, which may be ascribed to the coverage of the active site by degradation intermediates. To confirm this, the catalyst was heat-treated (calcined at 300 °C for 2 h) after the fourth cycle to remove the degradation intermediates adsorbed on the catalyst. As expected, the catalytic performance of Cu-CN was restored in the fifth cycle. Moreover, Fig. S17a shows that the Cu ion leaching in each cycle was maintained at a low concentration (< 0.21mgL-1), and after the first cycle, the Cu ion leaching decreased significantly, which is related to the loss and masking of Cu sites on the catalyst surface. After regeneration by heat treatment, the leaching amount of Cu ion is close to the first cycle, indicating that the surface Cu site can be re-exposed by heat treatment. Due to the leaching of Cu ion in

each cycle, the content of Cu in the catalyst regenerated by heat treatment after four cycles is slightly lower than that of the initial catalyst (from 15.46% to 14.89%) (Fig. S17b). FTIR spectra (Fig. S17c) shows that the basic skeleton structure of Cu-CN has no obvious change after heat treatment, only the characteristic peak of cyano group at 2180 cm^{-1} decreased [55], indicating that the edge cyano defects are reduced after regeneration. XPS spectra (Fig. S17d) shows that the proportion of Cu (II) in the regenerated catalyst increased, which is beneficial to the conversion of H_2O_2 to $^1O_2$ (Eq.3, Eq.4). These results indicated that Cu-CN has good stability and the catalytic performance can be regenerated by simple heat treatment.

3.8. Possible degradation pathways of MB in Cu-CN/H_2O_2

The degradation intermediates of MB in the Cu-CN/H_2O_2 system were determined by LC-MS chromatography and their structural formulae were deduced according to the relative molecular mass (Fig. S18, Table S5). The Fukui index was used to indicate the active center of MB molecule (Fig. S19a-c). A high f value means more vulnerable to electrophilic attack. According to the Fukui index results and the identified intermediates, the degradation pathways of MB can be speculated as follows. As shown in Fig. S19d, since S10 and N7 have the highest f values and are most easily oxidized by $^1O_2$ with electrophilic properties, S10 is oxidized by $^1O_2$ to form P1 first. Then N_7 is attacked by $^1O_2$, leading to the breakage of N_7-C_5 bond. At the same time, the Diels alder cycloaddition reaction occurs between C3 and C6 sites and $^1O_2$, which is converted to P2 by carbonylation. P2 can accept hydroxyl and further convert to P3 and P4. On the other hand, N15 and N16 with high f and f^{-0} values on MB can be demethylated by $^1O_2$ attack to form P5 and P6. P7 can be obtained from the oxidation of S in P6 by $^1O_2$, or from the oxidation of dimethylamine in P1 by $^1O_2$. P7 is oxidized to remove SO_2 to form P8. Subsequently, these intermediates undergo a series of hydroxylation, carbonylation and ring-opening oxidation to form small molecular intermediates (P9-P12), and finally gradually mineralized into CO_2 and H_2O over time. The analysis of the degradation pathways of MB reveals that $^1O_2$ plays an important role in the degradation of MB.

4. Conclusion

In summary, Cu single-atom catalyst with high-loaded Cu-N_3 sites can induce H_2O_2 to selectively generate $^1O_2$. Experimental and DFT calculation results reveal that Cu-N_3 structure and the high density of Cu-N_3 sites are the key factors for Cu-CN to induce H_2O_2 to selectively produce $^1O_2$. Furthermore, by adjusting the density of Cu-N_3 sites the catalytic pathway of Cu-CN/H_2O_2 Fenton-like system can be changed, with low Cu-N_3 sites density the contribution of ·OH increases, while high Cu-N_3 sites density favors $^1O_2$. Due to the nonradical oxidation pathway dominated by $^1O_2$, Cu-CN/H_2O_2 Fenton-like system can overcome the limitation of traditional H_2O_2-based Fenton-like catalytic systems and shows surprisingly high performance in the removal of organic pollution even under high salinity and alkaline conditions. Our work shows a highly efficient H_2O_2-based Fenton system for purifying high salinity and alkaline wastewater, revealing the potential of single-atom catalysts to activate H_2O_2 in nonradical pathways, and providing a reference for understanding its mechanism. We hope that our work can attract more researchers to study single-atom catalysts for nonradical activation of H_2O_2 and promote the application of H_2O_2-based Fenton-like in the purification of complex wastewater.

CRediT authorship contribution statement

Fuhang Xu: Conceptualization, Investigation, Methodology, Writing – original draft. **Cui Lai:** Funding acquisition, Resources, Methodology, Writing – review & editing. **Mingming Zhang:** Data curation, Formal analysis. **Bisheng Li:** Methodology, Writing – review & editing. **Ling Li:** Investigation, Methodology. **Shiyu Liu:** Methodology. **Dengsheng Ma:** Conceptualization, Software. **Xuerong Zhou:** Validation. **Huchuan Yan:** Supervision. **Xiuqin Huo:** Software. **Biting Wang:** Investigation. **Huan Yi:** Funding acquisition. **Lei Qin:** Resources. **Lin Tang:** Software.

Declaration of Competing Interest

The authors declare that they have no known competing financial interests or personal relationships that could have appeared to influence the work reported in this paper.

Data Availability

No data was used for the research described in the article.

Acknowledgement

This study was financially supported by the Program for the National Natural Science Foundation of China (52170161, 52100183), the Hunan Natural Science Foundation (2020JJ3009, 2022JJ40044), the Hunan Researcher Award Program (2020RC3025), the Project funded by China Postdoctoral Science Foundation (2021M700041), the Changsha Municipal Natural Science Foundation (kq2202166), Hunan Provincial Innovation Foundation for Postgraduate (CX20220422).

Appendix A. Supporting information

Supplementary data associated with this article can be found in the online version at doi:10.1016/j.apcatb.2023.123075.

References

[1] S.S. Chan, K.S. Khoo, K.W. Chew, T.C. Ling, P.L. Show, Recent advances biodegradation and biosorption of organic compounds from wastewater: microalgae-bacteria consortium-A review, Bioresour. Technol. 344 (2022), 126159.
[2] Y. Fu, Z. Yin, L. Qin, D. Huang, H. Yi, X. Liu, S. Liu, M. Zhang, B. Li, L. Li, W. Wang, X. Zhou, Y. Li, G. Zeng, C. Lai, Recent progress of noble metals with tailored features in catalytic oxidation for organic pollutants degradation, J. Hazard. Mater. 422 (2022), 126950.
[3] M. Zhou, J. Chen, S. Yu, B. Chen, C. Chen, L. Shen, B. Li, H. Lin, The coupling of persulfate activation and membrane separation for the effective pollutant degradation and membrane fouling alleviation, Chem. Eng. J. 451 (2023), 139009.
[4] J.K. An, N. Li, Y. Wu, S. Wang, C.M. Liao, Q. Zhao, L.A. Zhou, T. Li, X. Wang, Y. J. Feng, Revealing decay mechanisms of H2O2-Based electrochemical advanced oxidation processes after long-term operation for phenol degradation, Environ. Sci. Technol. 54 (2020) 10916–10925.
[5] D.B. Miklos, C. Remy, M. Jekel, K.G. Linden, J.E. Drewes, U. Hubner, Evaluation of advanced oxidation processes for water and wastewater treatment - A critical review, Water Res. 139 (2018) 118–131.
[6] C. Lai, H.C. Yan, D.B. Wang, S.Y. Liu, X.R. Zhou, X.P. Li, M.M. Zhang, L. Li, Y.K. Fu, F.H. Xu, X.F. Yang, X.Q. Huo, Facile synthesis of Mn, Ce co-doped g-C_3N_4 composite for peroxymonosulfate activation towards organic contaminant degradation, Chemosphere 293 (2022), 133472.
[7] M.P. Rayaroth, C.T. Aravindakumar, N.S. Shah, G. Boczkaj, Advanced oxidation processes (AOPs) based wastewater treatment - unexpected nitration side reactions-a serious environmental issue: a review, Chem. Eng. J. 430 (2022), 133002.
[8] Y.P. Zhu, R.L. Zhu, Y.F. Xi, J.X. Zhu, G.Q. Zhu, H.P. He, Strategies for enhancing the heterogeneous Fenton catalytic reactivity: a review, Appl. Catal. B-Environ. 255 (2019), 117739.
[9] B. Li, S. Liu, C. Lai, G. Zeng, M. Zhang, M. Zhou, D. Huang, L. Qin, X. Liu, Z. Li, N. An, F. Xu, H. Yi, Y. Zhang, L. Chen, Unravelling the interfacial charge migration pathway at atomic level in 2D/2D interfacial Schottky heterojunction for visible-light-driven molecular oxygen activation, Appl. Catal. B-Environ. 266 (2020), 118650.
[10] W. Ren, C. Cheng, P.H. Shao, X.B. Luo, H. Zhang, S.B. Wang, X.G. Duan, Origins of electron-transfer regime in persulfate-based nonradical oxidation processes, Environ. Sci. Technol. 56 (2022) 78–97.
[11] S. Liu, C. Lai, X. Zhou, C. Zhang, L. Chen, H. Yan, L. Qin, D. Huang, H. Ye, W. Chen, L. Li, M. Zhang, L. Tang, F. Xu, D. Ma, Peroxydisulfate activation by sulfur-doped ordered mesoporous carbon: insight into the intrinsic relationship between defects and $^1O_2$ generation, Water Res. 221 (2022), 118797.
[12] J.W. Pan, B.Y. Gao, Y. Gao, P.J. Duan, K.Y. Guo, M. Akram, X. Xu, Q.Y. Yue, In-situ Cu-doped carbon-supported catalysts applied for high-salinity polycarbonate plant wastewater treatment and a coupling application, Chem. Eng. J. 416 (2021), 129441.

[13] J.W. Pan, B.Y. Gao, P.J. Duan, K.Y. Guo, M. Akram, X. Xu, Q.Y. Yue, Y. Gao, Improving peroxymonosulfate activation by copper ion-saturated adsorbent-based single atom catalysts for the degradation of organic contaminants: electron-transfer mechanism and the key role of Cu single atoms, J. Mater. Chem. A 9 (2021) 11604–11613.

[14] C.T. Guan, J. Jiang, C.W. Luo, S.Y. Pang, Y. Yang, Z. Wang, J. Ma, J. Yu, X. Zhao, Oxidation of bromophenols by carbon nanotube activated peroxymonosulfate (PMS) and formation of brominated products: comparison to peroxydisulfate (PDS), Chem. Eng. J. 337 (2018) 40–50.

[15] Y. Shang, X. Xu, B. Gao, S. Wang, X. Duan, Single-atom catalysis in advanced oxidation processes for environmental remediation, Chem. Soc. Rev. 50 (2021) 5281–5322.

[16] M. Qian, X.L. Wu, M. Lu, L. Huang, W. Li, H. Lin, J. Chen, S. Wang, X. Duan, Modulation of charge trapping by island-like single-atom cobalt catalyst for enhanced photo-fenton-like reaction, Adv. Funct. Mater. 33 (2023) 2208688.

[17] S. Liu, D. Liu, Y. Sun, P. Xiao, H. Lin, J. Chen, X.-L. Wu, X. Duan, S. Wang, Enzyme-mimicking single-atom FeN_4 sites for enhanced photo-Fenton-like reactions, Appl. Catal. B-Environ. 310 (2022), 121327.

[18] F. Chen, X.L. Wu, C. Shi, H. Lin, J. Chen, Y. Shi, S. Wang, X. Duan, Molecular engineering toward pyrrolic N-Rich M-N_4 (M = Cr, Mn, Fe, Co, Cu) single-atom sites for enhanced heterogeneous fenton-like reaction, Adv. Funct. Mater. 31 (2021) 2007877.

[19] X.L. Wu, S. Liu, M. Yan, H. Lin, J. Chen, S. Liu, S. Wang, X. Duan, Directional and ultrafast charge transfer in oxygen-vacancy-rich ZnO@Single-Atom cobalt core-shell junction for photo-fenton-like reaction, Angew. Chem. Int. Ed. Engl. (2023), e202305639.

[20] L.X. Yang, H.Q. Yang, S.Y. Yin, X.Y. Wang, M.W. Xu, G.L. Lu, Z.N. Liu, H. Sun, Fe single-atom catalyst for efficient and rapid fenton-like degradation of organics and disinfection against bacteria, Small 18 (2022).

[21] Y. Xiong, H.C. Li, C.W. Liu, L.R. Zheng, C. Liu, J.O. Wang, S.J. Liu, Y.H. Han, L. Gu, J.S. Qian, D.S. Wang, Single-Atom Fe catalysts for fenton-like reactions: roles of different N species, Adv. Mater. 34 (2022).

[22] Y. Zhao, H. Zhou, X. Zhu, Y. Qu, C. Xiong, Z. Xue, Q. Zhang, X. Liu, F. Zhou, X. Mou, W. Wang, M. Chen, Y. Xiong, X. Lin, Y. Lin, W. Chen, H.-J. Wane, Z. Jiang, L. Zheng, T. Yao, J. Dong, S. Wei, W. Huang, L. Gu, J. Luo, Y. Li, Y. Wu, Simultaneous oxidative and reductive reactions in one system by atomic design, Nat. Catal. 4 (2021) 134–143.

[23] S. Zuo, X. Jin, X. Wang, Y. Lu, Q. Zhu, J. Wang, W. Liu, Y. Du, J. Wang, Sandwich structure stabilized atomic Fe catalyst for highly efficient Fenton-like reaction at all pH values, Appl. Catal. B-Environ. 282 (2021), 119551.

[24] J.F. Yu, H.P. Feng, L. Tang, Y. Pang, G.M. Zeng, Y. Lu, H.R. Dong, J.J. Wang, Y. N. Liu, C.Y. Feng, J.J. Wang, B. Peng, S.J. Ye, Metal-free carbon materials for persulfate-based advanced oxidation process: Microstructure, property and tailoring, Prog. Mater. Sci. 111 (2020), 100654.

[25] Z.C. Yang, J.S. Qian, A.Q. Yu, B.C. Pan, Singlet oxygen mediated iron-based Fenton-like catalysis under nanoconfinement, P. Natl. Acad. Sci. USA 116 (2019) 6659–6664.

[26] L. Li, Z. Yin, M. Cheng, L. Qin, S. Liu, H. Yi, M. Zhang, Y. Fu, X. Yang, X. Zhou, G. Zeng, C. Lai, Insights into reactive species generation and organics selective degradation in Fe-based heterogeneous Fenton-like systems: a critical review, Chem. Eng. J. 454 (2023), 140126.

[27] L. Li, S. Liu, M. Cheng, C. Lai, G. Zeng, L. Qin, X. Liu, B. Li, W. Zhang, Y. Yi, M. Zhang, Y. Fu, M. Li, M. Long, Improving the Fenton-like catalytic performance of MnOx-Fe3O4/biochar using reducing agents: A comparative study, J. Hazard. Mater. 406 (2021), 124333.

[28] L.S. Zhang, X.H. Jiang, Z.A. Zhong, L. Tian, Q. Sun, Y.T. Cui, X. Lu, J.P. Zou, S. L. Luo, Carbon nitride supported high-loading Fe single-atom catalyst for activation of peroxymonosulfate to generate $^1O_2$ with 100% selectivity, Angew. Chem. Int. Ed. Engl. 60 (2021) 21751–21755.

[29] X. Mi, P. Wang, S. Xu, L. Su, H. Zhong, H. Wang, Y. Li, S. Zhan, Almost 100% peroxymonosulfate conversion to singlet oxygen on single-atom CoN(2+2) sites, Angew. Chem. Int. Ed. Engl. 60 (2021) 4588–4593.

[30] S. Zuo, Z. Guan, F. Yang, D. Xia, D. Li, Reactive oxygen species regulation and synergistic effect for effective water purification through Fenton-like catalysis on single-atom Cu–N sites, J. Mater. Chem. A 10 (2022) 10503–10513.

[31] X. Lu, S. Gao, H. Lin, L. Yu, Y. Han, P. Zhu, W. Bao, H. Yao, Y. Chen, J. Shi, Bioinspired copper single-atom catalysts for tumor parallel catalytic therapy, Adv. Mater. 32 (2020), e2002246.

[32] X. Gao, W. Ma, J. Mao, C.T. He, W. Ji, Z. Chen, W. Chen, W. Wu, P. Yu, L. Mao, A single-atom Cu-N_2 catalyst eliminates oxygen interference for electrochemical sensing of hydrogen peroxide in a living animal brain, Chem. Sci. 12 (2021) 15045–15053.

[33] J. Gao, Hb Yang, X. Huang, S.-F. Hung, W. Cai, C. Jia, S. Miao, H.M. Chen, X. Yang, Y. Huang, T. Zhang, B. Liu, Enabling direct H_2O_2 production in acidic media through rational design of transition metal single atom catalyst, Chem 6 (2020) 658–674.

[34] X.D. Xiao, Y.T. Gao, L.P. Zhang, J.C. Zhang, Q. Zhang, Q. Li, H.L. Bao, J. Zhou, S. Miao, N. Chen, J.Q. Wang, B.J. Jiang, C.G. Tian, H.G. Fu, A promoted charge separation/transfer system from Cu single atoms and C_3N_4 layers for efficient photocatalysis, Adv. Mater. 32 (2020) 2003082.

[35] L. Chen, P. Guo, M. Qiao, S. Yan, H. Li, W. Shen, H. Xu, K. Fan, Cu/SiO_2 catalysts prepared by the ammonia-evaporation method: texture, structure, and catalytic performance in hydrogenation of dimethyl oxalate to ethylene glycol, J. Catal. 257 (2008) 172–180.

[36] J.L. Liang, Q.Q. Song, J.H. Wu, Q. Lei, J. Li, W. Zhang, Z.M. Huang, T.X. Kang, H. Xu, P. Wang, X.T. Zhou, P.K. Wong, H.M. Li, X.M. Meng, Z.F. Jiang, C.S. Lee, Anchoring copper single atoms on porous boron nitride nanofiber to boost selective reduction of nitroaromatics, ACS Nano 16 (2022) 4152–4161.

[37] B.Q. Wang, C. Cheng, M.M. Jin, J. He, H. Zhang, W. Ren, J. Li, D.S. Wang, Y.D. Li, A. Site, Distance effect induced by reactant molecule matchup in single-atom catalysts for fenton-like reactions, Angew. Chem. Int. Ed. 134 (2022), e202207268.

[38] P. Yang, Y. Long, W. Huang, D. Liu, Single-atom copper embedded in two-dimensional MXene toward peroxymonosulfate activation to generate singlet oxygen with nearly 100% selectivity for enhanced Fenton-like reactions, Appl. Catal. B-Environ. 324 (2023), 122245.

[39] M.M. Zhang, C. Lai, B.S. Li, F.H. Xu, D.L. Huang, S.Y. Liu, L. Qin, X.G. Liu, H. Yi, Y. K. Fu, L. Li, N. An, L. Chen, Insightful understanding of charge carrier transfer in 2D/2D heterojunction photocatalyst: Ni-Co layered double hydroxides deposited on ornamental g-C_3N_4 ultrathin nanosheet with boosted molecular oxygen activation, Chem. Eng. J. 422 (2021), 130120.

[40] X.R. Zhou, Z.T. Zeng, G.M. Zeng, C. Lai, R. Xiao, S.Y. Liu, D.L. Huang, L. Qin, X. G. Liu, B.S. Li, H. Yi, Y.K. Fu, L. Li, Z.H. Wang, Z.H. Wang, Insight into the mechanism of persulfate activated by bone char: unraveling the role of functional structure of biochar, Chem. Eng. J. 401 (2020), 126127.

[41] D.B. Tada, L.L.R. Vono, E.L. Duarte, R. Itri, P.K. Kiyohara, M.S. Baptista, L.M. Rossi, Methylene blue-containing silica-coated magnetic particles: a potential magnetic carrier for photodynamic therapy, Langmuir 23 (2007) 8194–8199.

[42] F. Chen, L.-L. Liu, J.-J. Chen, W.-W. Li, Y.-P. Chen, Y.-J. Zhang, J.-H. Wu, S.-C. Mei, Q. Yang, H.-Q. Yu, Efficient decontamination of organic pollutants under high salinity conditions by a nonradical peroxymonosulfate activation system, Water Res. 191 (2021), 116799.

[43] H. Li, J. Tian, F. Xiao, R. Huang, S. Gao, F. Cui, S. Wang, X. Duan, Structure-dependent catalysis of cuprous oxides in peroxymonosulfate activation via nonradical pathway with a high oxidation capacity, J. Hazard. Mater. 385 (2020), 121518.

[44] L. Yang, Z. Xiong, J. Li, Z. Wu, X. Zhao, C. Zhao, Y. Zhou, Y. Qian, B. Lai, Iron active sites encapsulated in N-doped graphite for efficiently selective degradation of emerging contaminants via peroxymonosulfate (PMS) activation: inherent roles of adsorption and electron-transfer dominated nonradical mechanisms, Chem. Eng. J. 444 (2022), 136623.

[45] X. Zhou, M.K. Ke, G.X. Huang, C. Chen, W. Chen, K. Liang, Y. Qu, J. Yang, Y. Wang, F. Li, H.Q. Yu, Y. Wu, Identification of Fenton-like active Cu sites by heteroatom modulation of electronic density, Proc. Natl. Acad. Sci. USA 119 (2022), e2119492119.

[46] F. Li, Z. Lu, T. Li, P. Zhang, C. Hu, Origin of the excellent activity and selectivity of a single-atom copper catalyst with unsaturated Cu-N_2 sites via peroxydisulfate activation: Cu(III) as a dominant oxidizing species, Environ. Sci. Technol. 56 (2022) 8765–8775.

[47] K.M. Khan AU, Singlet molecular oxygen in the Haber-Weiss reaction, Proc. Natl. Acad. Sci. USA 91 (1994) 12365–12367.

[48] K. WH, Reactions involving singlet oxygen and the superoxide anion, Nature 262 (1976) 420–421.

[49] J.W. Moffett, R.G. Zika, Reaction kinetics of hydrogen peroxide with copper and iron in seawater, Environ. Sci. Technol. 21 (1987) 804–810.

[50] J.D.La.H. Gallard, Catalytic decomposition of hydrogen peroxide by Fe(III) in homogeneous aqueous solution: mechanism and kinetic modeling, Environ. Sci. Technol. 33 (1999) 2726–2732.

[51] S. Foley, P. Rotureau, S. Pin, G. Baldacchino, J.P. Renault, J.C. Mialocq, Radiolysis of confined water: Production and reactivity of hydroxyl radicals, Angew. Chem. Int. Ed. 44 (2005) 110–112.

[52] L.A. MacManus-Spencer, K. McNeill, Quantification of singlet oxygen production in the reaction of superoxide with hydrogen peroxide using a selective chemiluminescent probe, J. Am. Chem. Soc. 127 (2005) 8954–8955.

[53] S.Q. Xu, H.X. Zhu, W.R. Cao, Z.B. Wen, J.N. Wang, C.P. Francois-Xavier, T. Wintgens, Cu-Al_2O_3-g-C_3N_4 and Cu-Al_2O_3-C-dots with dual-reaction centres for simultaneous enhancement of Fenton-like catalytic activity and selective H_2O_2 conversion to hydroxyl radicals, Appl. Catal. B-Environ. 234 (2018) 223–233.

[54] Y.X. Mao, J.L. Liang, L. Jiang, Q.S. Shen, Q. Zhang, C.C. Liu, H. Zheng, Y. Liao, X. K. Cao, H.Y. Dong, F.Y. Ji, Removal of micro organic pollutants in high salinity wastewater by comproportionation system of Fe(VI)/Fe(III): Enhancement of chloride and bicarbonate, Water Res. 214 (2022), 118182.

[55] Z. Zhu, H. Pan, M. Murugananthan, J. Gong, Y. Zhang, Visible light-driven photocatalytically active g-C_3N_4 material for enhanced generation of H_2O_2, Appl. Catal. B-Environ. 232 (2018) 19–25.